ACS OMEGA

Article

Cite This: ACS Omega 2019, 4, 1292−1299

http://pubs.acs.org/journal/acsodf

Reconstruction of Soil Components into Multifunctional Freestanding Membranes

Jumi Deka,[†,∥] Kundan Saha,[†,∥] Tukhar Jyoti Konch,[†] Raj Kumar Gogoi,[†] Subhasmita Saikia,[†] Partha Pratim Saikia,[‡] Gitish K. Dutta,[§] and Kalyan Raidongia*[,†]

[†]Department of Chemistry, Indian Institute of Technology Guwahati, Guwahati, 781039 Assam, India

[‡]Department of Chemistry, NNS College, Titabar, 785630 Assam, India

[§]Department of Chemistry, National Institute of Technology Meghalaya, 793003 Shillong, Meghalaya, India

Supporting Information

ABSTRACT: Multifunctional freestanding membranes are prepared by tuning the structure of ubiquitous soil components, viz. clay and humic acids. Cross-linking of exfoliated clay layers with purified humic acids not only conferred mechanical strength but also enhanced chemical robustness of the membranes. The percolated network of molecularly sized channels of the soil membranes exhibits characteristic nanofluidic phenomena. Electrical conductivity is induced to otherwise insulating soil membranes by heating in an inert atmosphere, without affecting their nanofluidic ionic conductivity. The soil membranes also provided a new platform to prepare and study mixed conducting materials. Strips of heated membranes are shown to exhibit excellent sensitivity toward NH_3 gas under atmospheric conditions.

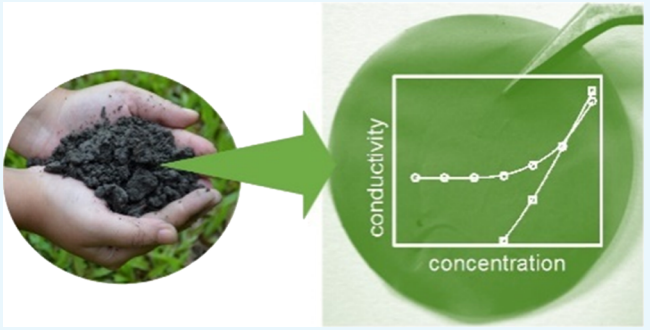

1. INTRODUCTION

Soil, also known as the skin of the earth, is a highly complicated but a synergic mixture of living and nonliving objects.[1,2] It plays pivotal roles in the environmental chemical cycles and provides a basis for the survival of life on earth. Among various nonliving objects in soil, clays and humic acids (HAs) are the most active constituents, and in spite of their drastically different chemical and physical identities, they contribute similarly to the chemical functionalities of soil. For example, both clays and HAs actively participate in detoxification of hazardous substances, preservation of vital minerals, and maintenance of ideal pH, fertility, and air/water ratios for plant growth.[1−6] Studies suggested that the activities of clay and HAs complement each other and an appropriate combination of the two is essential to obtain certain crucial functionalities of soil.[1−10] Nonetheless, rational blends of these two naturally abandoned materials have not been optimally applied with a view to creating advanced materials for futuristic applications. Here, we attempt to utilize the ubiquitous chemistry of HAs and clays to prepare multifunctional freestanding membranes with application possibilities in the areas like nanofluidic energy harvesting, water purification, and sensing of toxic chemicals. To facilitate better interactions, layers of naturally occurring vermiculite clay were exfoliated into ultrathin 2D sheets, and HAs were purified through multiple steps of conjugative acid−base treatments.

Clays are stacking layers of hydrous aluminum phyllosilicates consisting of corner-sharing SiO_4 tetrahedra and/or AlO_4 octahedra intercalated by aqueous solutions of charge-balancing cations. Owing to their well-defined structures having high chemical and thermal stability, clay minerals have received lots of attention from the scientific communities across the disciplines. As a result, they are being applied in a variety of advanced technologies such as nuclear waste managements, industrial oil absorbance, pharmaceuticals, and anticaking applications.[11] Clays are also highly tuneable and can be easily modified to create freestanding proton-conducting membranes, ultrasensitive smart materials, and a range of polymeric nanocomposites.[12−15] On the other hand, HAs are mixtures of acidic organic polymers that are believed to be a product of the natural break-down process of plant- and animal-based materials.[16,17] There have been significant contradictions regarding the origin and structure of HAs. However, their favorable contributions toward environmental chemical cycles have been proven beyond doubt. The phenolic and carboxylic functional groups of HAs together with negative surface charges of clay layers are the major contributors of the cation exchange capacity of soil, and hence, contents of the two are a primary characterization of soil nature. Unfortunately, the application of HAs in advanced technologies is limited by its complicated and undefined structures. They are being utilized as a cheap source of carbon, either to generate heat through

Received: November 11, 2018
Accepted: January 3, 2019
Published: January 15, 2019

DOI: 10.1021/acsomega.8b03144
ACS Omega 2019, 4, 1292−1299

combustion or to prepare porous materials by annealing at an inert atmosphere.[18,19] Scant efforts have been made to utilize the large number of functional groups inherently present in HAs for advanced technological applications. Notable applications of HAs include adsorbents of inorganic and organic pollutants from water and additives to fertilizer, paper, and plastic materials.[20−22]

2. RESULTS AND DISCUSSIONS

HAs, the mixtures of acidic organic polymers that are believed to be a product of the natural break-down process of plant- and animal-based materials,[16,17] were extracted and purified following the standard alkaline-acid treatment-based procedure.[23−25] The purified HA samples displayed infra-red (IR), UV−vis, and fluorescence spectra similar to those reported in the contemporary literature (see Figure S1).[25−28] IR bands at 3424, 2928, 1655, and 1030 cm^{-1} suggest the presence of −OH, −CH, −C═C, and C−O−C groups in the sample, respectively. Clays are stacking layers of hydrous aluminum phyllosilicates consisting of corner-sharing SiO_4 tetrahedra and/or AlO_4 octahedra intercalated by an aqueous solution of charge-balancing cations. Owing to their well-defined structures along with high chemical and thermal stability, clay minerals have received lots of attention from the scientific community across the disciplines. As a result, they are being applied in a variety of advanced technologies such as nuclear waste management, industrial oil absorbance, pharmaceuticals, and anticaking applications.[1,26] Natural vermiculite $(Al,Mg,Fe^{3+})_4(Si,Al)_8O_{20}(OH)_4$, a smectite group 2:1 clay, is used here as the model clay system; the X-ray diffraction (XRD) pattern of the same is shown in Supporting Information, Figure S1c.[1] A two-step ion exchange method was employed to obtain a homogeneous aqueous dispersion of the clay sample as shown in Figure S1a. The microscopic analysis of the dispersion (discussed on Figure S2) confirmed the successful exfoliation of clay layers into thin flakes having heights in the range of 4−8 nm with lateral dimensions extending up to 20 μm.[2]

Aqueous dispersions of exfoliated clay layers and purified HAs were mixed at different ratios and their colloidal stability was monitored over a period of 3 months. Pure HAs and vermiculite dispersions started settling down after around 24 undisturbed hours; in contrast, HA−vermiculite dispersions remain stable up to 3 months, indicating favorable interactions between the two; photos of the dispersions are compared in Figure 1a,b. Such augmentations of colloidal stability of bulk clay particles induced by HAs are already documented in the relevant literature.[1,29−32] HAs bind to clay particles through the following modes of interactions—(a) anion exchange to clay edges, (b) cation- or water-bridges to clay surfaces, (c) H-bonding to the surface Si−OH groups, and (d) van der Waals forces. Although unbound hydrophilic side chains of HAs assist dispersion of clay particles in water, the surface charges of clay layers prevent agglomeration of HAs into polymeric particles. Exfoliation of bulk clay particles into nanoflakes increases not only surface-to-volume ratios but also the number of defect sites necessary to interact with HAs. Similarly, multiple steps of purification should free more functional groups in HA to interact with clay layers, and hence, a pronounced cross-linking between the two is expected. A hypothetical model depicting interactions between HA functional groups and silica sheets of exfoliated clay layers is shown in Scheme 1.

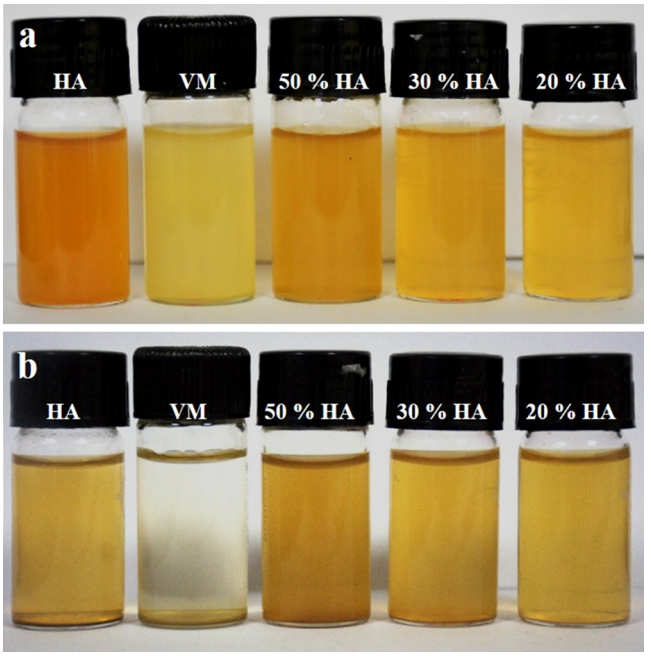

Figure 1. Photographs showing aqueous dispersions of HA, VM, 20% HA, 30% HA, and 50% HA at (a) day 1 and (b) day 90.

Scheme 1. Schematic Showing Probable Interactions of HA Functional Groups with Silicate Sheets of Exfoliated Vermiculite Layers

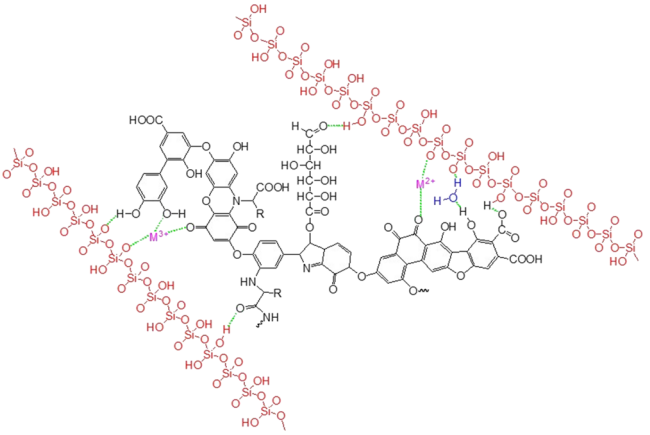

The diverse cross-linking possibilities of HAs and exfoliated clay layers should yield highly robust composite materials. Seeking a proof of this concept, dispersions of HAs and exfoliated vermiculite layers were mixed in different weight ratios (20, 30, 50, and 70% HAs) and vacuum-filtrated through commercial filtration membranes to obtain freestanding membranes. A photo of the as-prepared membrane containing 50% HA (50% HA) is shown in Figure 2a. Soil composites up to 50% HA contents gave highly robust freestanding membranes, but the composite with higher than 50% HA yielded fragile membranes, which tend to break easily and hence not considered for future applications. Field emission scanning electron microscopy (FESEM) examination on the cross section of the soil membrane revealed its lamellar structure; a representative image of the same is shown in Figure 2b. The lamellar structures of membranes are also supported by the presence of reflections in the range of 2θ = 6.5°−5.8°, in their respective powder XRD patterns (Figure

DOI: 10.1021/acsomega.8b03144
ACS Omega 2019, 4, 1292−1299

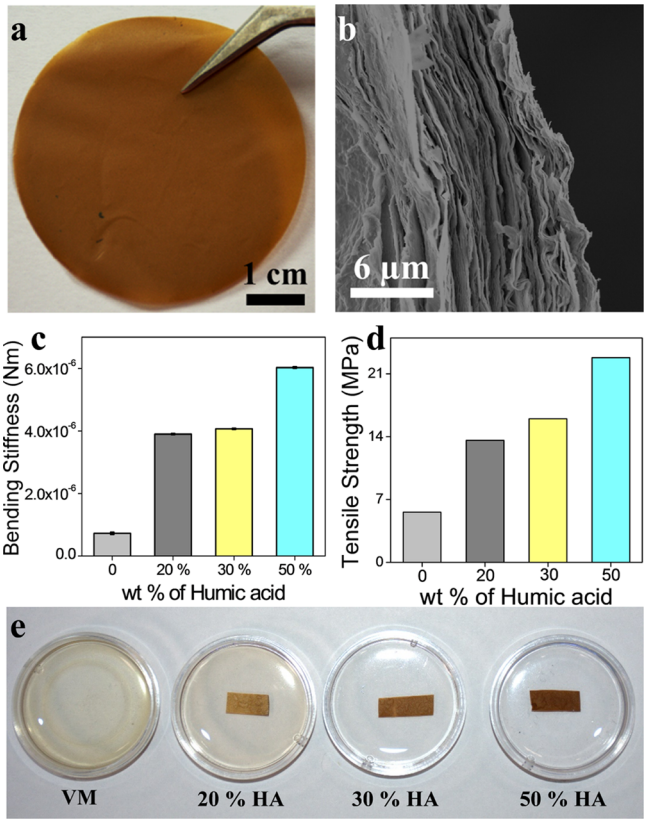

Figure 2. Freestanding soil membranes: (a) digital photo and (b) cross-sectional FESEM image of the soil membrane containing 50% HA (50% HA). (c) Bending stiffness and (d) tensile strength of soil membranes with different compositions. (e) Photographs showing solution stability of soil membranes dipped in water for 30 days after 2 h of shaking.

S3). The interlayer spacing of the soil membranes calculated by applying Bragg's law was found to be in the range of 1.2−1.6 nm. The bar diagrams in Figure 2c show bending stiffness values of the membranes calculated by the Lorentzen & Wettre two-point method,[14,33] described in Figure S4. The stiffness values of the soil membranes were found to increase with increasing HA content in it. The cross-linking of exfoliated vermiculite with HA functional groups should prevent the sliding of vermiculite sheets from their specific position, resulting in higher values of stiffness. The stiffness of the soil membranes was found to be also dependent on the atmospheric humidity level or presence of solvent vapors. As described in the Supporting Information (Figure S5a), in the presence of acetone and ethanol, the stiffness of the membranes decreases, but it increases with increasing humidity level in the atmosphere (Figure S5b). The synergic effect of HAs and exfoliated clay layers was also established by comparing the tensile strength values of the soil membranes with that of a pure vermiculite membrane (Figure 2d). While the tensile strength values of 20, 30, and 50% HA membranes were found to be 2.4, 3, and 4 times higher than that of a pure vermiculite membrane, respectively, pure HAs did not yield any membrane upon vacuum filtration. The higher tensile strength values of soil membranes over pure vermiculite membranes can also be attributed to the cross-linking effect (Scheme 1) of HAs. The cross-linker prevents sliding of the vermiculite sheets from their specific position to improve the mechanical properties. However, in the membranes with higher than 50% HAs, the cross-linker dominates over vermiculite fractions of the composites and hence the tensile strength values follow the opposite trends. For the same reason, soil samples with HA content significantly higher than that of the two-dimensional vermiculite flakes do not yield freestanding membranes. The stress−strain curve of the composite membranes is compared with that of a pure vermiculite membrane in Figure S6. Cross-linking of clay layers by HAs also fetched extraordinary underwater stability to the soil membranes. To verify underwater stability in a realistic condition, small pieces (20 mm × 4 mm × 0.045 mm) of membranes were dipped into water and vigorously shaken for 2 h. While the pristine vermiculite membrane was disintegrated into an aqueous dispersion within 10 min of shaking, all composite membranes remained unperturbed. Figure 2e shows photos of the soil membranes that survived for 30 days in water after 2 h of vigorous shaking. Membranes with high solution stability are vital for applications like water purification, fuel cells, nanofluidics, and solution-based catalysis. Involvement of surface −OH groups on the cross-linking process is also supported by the diminishing intensity of the IR band corresponding to −OH groups in the composite membranes as compared to that of purified HAs and exfoliated vermiculite samples, shown in Figure S7.

Distinct XRD reflections at the low-angle region of the soil membranes indicate periodic stacking of the layers with well-defined interlayer spacing. Such minuscule spaces in the 1−2 nm regime decorated with diverse organic and inorganic functional groups should exhibit unique molecular and/or ionic transport properties. Soil-based nanofluidic devices were fabricated by encapsulating rectangular soil strips into a freshly prepared polydimethylsiloxane (PDMS) elastomer, see Experimental Section. In Figure 3a, current versus voltage ($I-V$) curves recorded with the soil-based nanofluidic device (50% HA) with three different KCl concentrations are plotted. The linearity in the $I-V$ curves confirmed the formation of a percolated network of nanofluidic channels across the soil membrane. Conductivity values of the nanofluidic devices were calculated from the respective $I-V$ curves at different salt concentrations and were compared with bulk electrolyte solutions. As can be seen from Figure 3b, the conductivity of the bulk solution varies linearly with concentration. In a clear contrast, conductivity of the soil membranes exhibits two distinct features. At high concentrations, it increases linearly with increasing salt concentrations, but for the salt concentrations below 0.1 M, conductivity remains unperturbed even after several orders of magnitude change in the concentration (from 0.1 to 10^{-6} M). This behavior of concentration-dependent ionic conductivity, also known as surface charge-governed ionic transport, is a characteristic signature of nanofluidic channels.[12,34] Nanofluidic membranes exhibiting surface charge-governed ionic transport up to 0.1 M salt concentration along with ease of fabrication and scaling up could be suitable for various technological applications. Soil-based nanofluidic membranes are also employed to harvest green energy from concentration differences. For that, devices comprising two compartments separated by a soil membrane were fabricated by using the PDMS elastomer, shown in the Figure S8a,b. Both compartments were filled with 2 mL of aqueous KCl solutions of different concentrations, 1 M in the high- (C_H) and 10^{-3} M in the low (C_L)-concentration chamber. Two Ag/AgCl electrodes were inserted into the electrolyte solutions to measure the transmembrane potentials

DOI: 10.1021/acsomega.8b03144
ACS Omega 2019, 4, 1292−1299

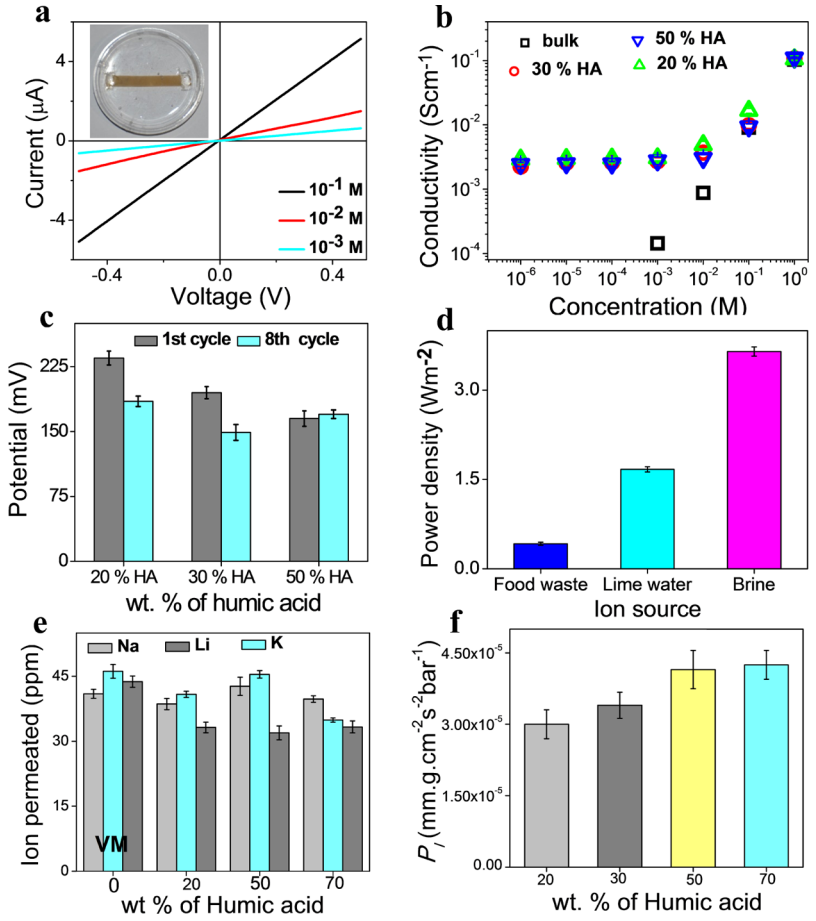

Figure 3. Nanofluidic characteristics of soil membranes: (a) representative $I-V$ curves obtained with a soil-based nanofluidic device at different KCl concentrations (b) ionic conductivity as a function of KCl concentration for different soil-based nanofluidic devices and bulk solution. (c) Trans-membrane potential of soil membranes placed between electrolytes with 3 orders of concentration difference for the 1st and 8th cycle. (d) Power harvested from naturally available ion sources by employing a 50% HA membrane-based nanofluidic device. Bar diagrams showing (e) ion permeation efficiency of soil membranes. (f) Permeability of liquids through different soil membranes.

and diffusion currents across the soil membranes. The transmembrane potentials recorded as a function of time for different soil membranes are shown in Figure S8c. Immediately after applying the concentration gradient, each of the devices displayed a maximum open-circuit potential which declined with time to reach equilibrium at around 0.22, 0.19, and 0.15 V for 20, 30, and 50% HA membranes, respectively. Such potential differences obtained through nanofluidic membranes are attributed to the concentration gradient-driven selective cation transport across the membranes.[35] The equilibrium power outputs across the membranes were calculated by using eq 1 to be 2.85, 1.46, and 1.2 W m^{-2} for 20, 30, and 50% HA, respectively, which are around 50% higher than those reported earlier for graphene oxide membranes.[36]

$$P_{max} = \frac{V_m \times I_0}{A} \quad (1)$$

where V_m and I_0 are the membrane potential and zero-volt current, respectively, and A is the diffusive membrane area. The stability in power output by soil membranes was ascertained by repeating the experiment several times, and the transmembrane potentials obtained on 1st and 8th cycle are shown as a function of the HA content in Figure 3c. Soil membranes displayed remarkably high cation transference numbers 1.00, 0.94, and 0.97 for the 20, 30, and 50% HA membrane, respectively, calculated by using eq 2.

$$E_{diff} = (2t_+ - 1)\frac{RT}{zF}\ln\frac{C_H}{C_L} \quad (2)$$

where, E_{diff} is the stable membrane potential of the device at 8th run, R is the universal gas constant, T is the room temperature, z is the no. of moles of electrons, F is the Faraday constant, and C_H and C_L are the concentration of the salt solution at high- and low-concentration chamber, respectively. As the stability of the soil membranes plays a vital role in these kinds of applications, the stability of soil membranes in energy-harvesting devices was evaluated by exposing the same to electrolyte solutions for several days. The device composed of the pure vermiculite membrane collapsed within 12 h, whereas the devices composed of composite membranes remained stable up to 10 days as demonstrated in Figure S10. Soil membranes were also tested for harvesting green energy from natural ion sources such as food waste, lime juice, and simulated seawater. Figure 3d shows power obtained by adding natural ion sources to the high-concentration chamber while filling the low concentration chamber with deionized water.

The molecularly thin nanofluidic channels of soil membranes enriched with surface charges also enable the selective cation transport behavior. Aqueous solutions (50 ppm) of

DOI: 10.1021/acsomega.8b03144
ACS Omega 2019, 4, 1292−1299

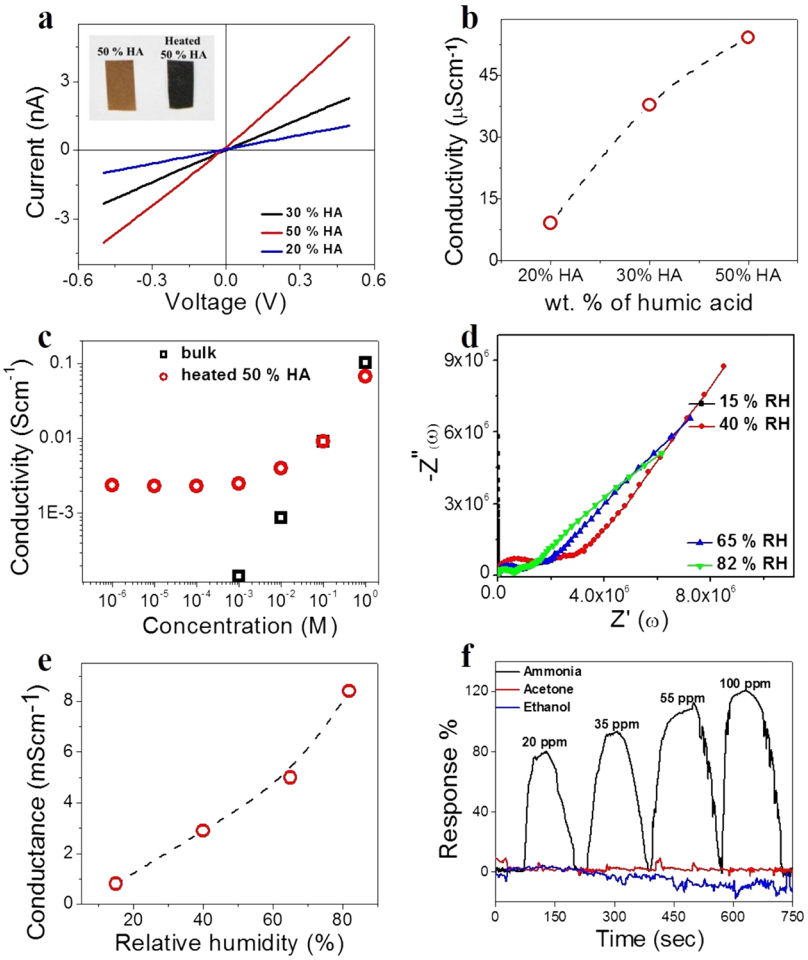

Figure 4. Heated soil membranes: (a) characteristic $I-V$ curves of soil membranes heated up to 550 °C under a N_2 atmosphere. (b) Electrical conductivity of the membranes as a function of HA contents in the initial mixture. (c) Surface charge-governed ionic conductivity of the heated soil membrane (50% HA). (d) Representative Cole−Cole plots for the heated membrane at different RHs. (e) Total conductivity as a function of RH. (f) Response curve for a heated 50% HA strip toward different concentrations of ammonia vapor is compared with that of acetone and ethanol vapors.

NaCl, KCl, and LiCl were vacuum-filtered through composite membranes (thickness 44 microns), and the concentration of the cations in the filtrate was determined by using a flame-photometer instrument. The bar diagrams in Figure 3e, showing concentrations of the cations permeated through the composite membranes, clearly illustrate the ion-selective nature of the membrane. For example, through the 70% HA membrane, a K^+ ion with a hydration radius of 3.3 Å was transported 2 and 3 times higher than that of Na^+ and Li^+ ions with hydration radii of 3.6 and 3.8 Å, respectively. The same trend of ion permeation was also followed by 20, and 50% HA membranes. In spite of smaller interlayer spacing (d = 1.37 nm), the pure vermiculite membrane did not show notable selectivity toward any particular cations. The rich chemical functionalities of HAs in the soil membranes are also utilized to separate cationic dyes from aqueous solutions. To investigate the efficiency of dye separation, 60 mL solutions of 100 ppm methylene blue (MB) dye were passed through soil membranes (30 μm), and the concentrations of the dye molecules were measured before and after passing through each membrane by employing UV−visible spectroscopy. The soil membranes could easily remove up to 60 mg of the dye molecule as illustrated in Figure S9. Remarkably, soil membranes exhibit much higher removal efficiency under vacuum-assisted filtration than its absorption capacity, by dipping the membranes in the dye solution. A 50% HA membrane (weight 10 mg) could remove up to 61.2 mg of MB dye under the vacuum filtration method, while it could absorb only 12.24 mg when soaked in an aqueous dye solution of similar concentrations for 2 h, suggesting the same to be a filtration process and not absorption. From the time required to vacuum-filter the dye solution, the liquid permeability of the soil membranes of different compositions was calculated. As shown in the bar diagram of Figure 3f, the permeability of the 70% HA membrane (4.25×10^{-5} mm g cm^{-2} s^{-1} bar^{-1}) was found to be slightly higher than that of other membranes.

As both HAs and clay are electrically nonconducting, pristine soil membranes are insulating in nature. However, electronic conductivity has been induced to the soil membranes by heating them under a N_2 atmosphere. Figure 4a shows the $I-V$ curve of the heated strips measured by painting conductive silver paste on either end. Moreover, conductivities of the heated soil membranes were found to be linearly dependent on the HA contents in the starting mixture, see Figure 4b. The electrical conductivities obtained as such are attributed to the removal of the organic functional groups from HAs during the heat treatment process, which is also apparent from the color transformation of soil strips from

DOI: 10.1021/acsomega.8b03144
ACS Omega 2019, 4, 1292−1299

brown to black; digital photos of a 50% HA strip before and after annealing at 550 °C is shown in the inset of Figure 4a. Also, the appearance of a G band in the Raman spectra of heat-treated soil strips, shown in Figure S11, suggests the enhancement of graphitic/amorphous carbon ratios in the samples, which can lead to a continuous network of graphitic carbon in the sample. The removal of organic functional groups from HA on heat treatment is further supported by comparing the IR spectra of the heated HA with that of the preheated HA as shown in Figure S12. The conversion of the carboxyl functionality is demonstrated by the disappearance of a sharp carbonyl peak at 1653 cm^{-1}. The heat treatment also reduced the interlayer spacing of soil membranes from 1.6 to 1.29 nm, shown in Figure S13. A characteristic $I-V$ curve of the heated pure HA shown in Figure S14 confirms the induction of electrical conductivity in heated HA. At present, the electrical conductivity of the heated soil samples is very low. However, for applications like chemical sensing or biosensing, more than higher values of conductivity, higher change in conductivity (with respect to change in the external atmosphere) is important. Moreover, tuning the composition and annealing temperature can further improve conductivity of the soil membranes. It is noteworthy that the high-temperature annealing process that fetched electrical conductivity to the soil strips did not affect its nanofluidic ionic conductivity. The residual functional groups of soil components are found to be sufficient to exhibit surface charge-governed ionic transport as shown in Figure 4c. Systems with such interpenetrating ionic and electronic conductivity have large potential for technological applications. The mixed conducting properties of heated soil strips were studied by measuring the conductivity at different relative humidity (RH) by employing an impedance analyzer (Multi Autolab/M204 potentiostat/galvanostat equipped with a FRA32M module) in the frequency range from 500 kHz to 1 Hz, with a perturbation voltage amplitude of 100 mV. Representative Cole−Cole plots obtained for the device made from the heated soil strip at different RHs are shown in Figure 4d. Total conductivities (σ) of the membrane were calculated by using the formula $\sigma = L/(R \times A)$, where L is the distance between the two electrodes and A is the cross-sectional area of the strip. The alternating current impedances (R) were obtained by fitting the data of the Cole−Cole plot to an equivalent circuit shown in Figure S15; a similar device geometry and equivalent circuit have been employed earlier to study mixed conducting properties of graphene oxide-reduced graphene oxide-based membranes.[37] As shown in Figure 4e, total conductivity decreases with decreasing RH of the atmosphere, suggesting ionic (proton) conductivity as a major contributor to the overall conductivity of the heated soil strips.

Freestanding mixed conducting membranes prepared from low-cost starting materials with tunable electrical conductivity could be ideal for gas sensing applications. A soil-based gas-sensing device was fabricated by connecting two Cu wires to silver paste painted on both ends of a rectangular soil strip (50% HA) of dimensions 20 mm × 6 mm × 0.045 mm. The soil device thus prepared was placed in a closed aluminum container as illustrated in the schematic of Figure S16. The electrical resistance of the same was recorded as a function of time using a source meter instrument. Calculated amounts of ammonia vapor were introduced into the chamber through a liquid injection syringe. The real-time response curve recorded for the heated soil membrane at four different concentrations of NH_3 vapor is shown in Figure 4f. The heated soil membrane showed 80% responsiveness toward 20 ppm of ammonia vapors. The high sensitivity of the heated soil membrane toward ammonia vapors can be attributed to smaller flake sizes, higher defect density, and larger interlayer spacing. However, under similar conditions, the heated soil membrane did not show any sensitivity toward ethanol and acetone vapors.

3. CONCLUSIONS

The work here demonstrated that naturally abundant soil components can be engineered to prepare advanced materials for futuristic applications. Clay layers exfoliated by ion-exchange methods were cross-linked by purified HA molecules to yield mechanically robust soil membranes possessing great potential toward solution-based applications. The percolated network of the ultrathin nanochannel exhibiting fascinating transport properties could find applications in the areas of selective molecular/ionic transport, catalysis, energy harvesting, and storage. The interpenetrating ionic and electronic conductivities of heated soil membranes prepared from dirt cheap raw materials by employing a straightforward and scalable method could provide a new platform to study mixed conducting materials. Such materials could be ideal in the areas like solid-state fuel cells, batteries, and supercapacitors, gas sensing, and separation. Exhaustive investigations into various ways of tuning soil chemistry may also provide means to alter the quality of the soil in natural environments.

4. EXPERIMENTAL SECTION

4.1. Materials. Raw vermiculite crystals, potassium chloride, and MB were purchased from Sigma-Aldrich. Sodium hydroxide, sodium chloride, and lithium chloride were purchased from Alfa Aesar. Hydrochloric acid and ammonium solution were purchased from Merck.

4.2. Exfoliation of Clay Layers. Natural vermiculite clay was exfoliated into atomically thin flakes by employing a two-step ion-exchange method. Typically, 50 mg of thermally expanded vermiculite crystals was refluxed with 100 mL of saturated solution of NaCl for 24 h, followed by washing with deionized water (DI water) 5−6 times. The as-obtained Na^+ ion-exchanged clay was further refluxed with 2 M aqueous solution of LiCl (100 mL) for 24 h. Li^+ ion-exchanged vermiculite was vigorously washed with DI water (5−6 times) to remove the free ions.

4.3. Extraction of HAs. A two-step alkaline-acid treatment was adopted to extract HA from samples of soil collected from the IITG campus. Typically, 100 g of the soil sample was stirred with 300 mL of 0.1 M aqueous NaOH solution at room temperature for 2 h. The soil components were then allowed to settle overnight and the supernatant liquid (200 mL) was collected, which was further centrifuged (5000 rpm) to confirm removal of undesired components. The clear solution was then acidified with concentrated HCl to decrease the pH value to 1. At pH 1, a brown-colored material started precipitating, which was collected by centrifugation and the washing procedure was repeated.

4.4. Preparation of Soil Membranes. Aqueous dispersions (1 mg/mL) of exfoliated vermiculite and HAs were mixed in appropriate proportions to prepare soil dispersions containing 20, 30, 50, and 70% of HAs by weight. For example to prepare 60 mL, 20% HA membrane, 12 mL of HA dispersion (1 mg/mL) was mixed with 48 mL of VM

DOI: 10.1021/acsomega.8b03144
ACS Omega 2019, 4, 1292−1299

dispersion (1 mg/mL) and sonicated for 5 min. Around 60 mL of soil dispersions was then vacuum-filtered through cellulose nitrate membranes to prepare freestanding membranes, which were detached from the filtration membranes after air-drying at room temperature.

4.5. Fabrication of the Nanofluidic Device. Soil membrane-based nanofluidic devices were fabricated by encapsulating rectangular soil strips (20 mm × 8 mm × 0.045 mm) into the freshly prepared PDMS elastomer. To expose the nanochannel networks to different electrolyte solutions, two holes (~0.3 mL) were cut open through the fully cured PDMS stub at either end of rectangular strips. After soaking soil devices in water for 8 h, aqueous solutions of KCl (~0.3 mL) were placed at both ends and allowed to reach equilibrium before measuring ionic conductance. A Keithley source meter instrument (model 2450) connected to Ag/AgCl electrodes was employed to record the conductivity data.

4.6. Cation and Dye Filtration through Soil Membranes. Hundred ppm and fifty ppm aqueous solutions (4 mL) of MB dye and inorganic salts were passed through soil membranes by a vacuum-assisted filtration technique, respectively. Aqueous dye solutions (100 ppm) (4 mL) were passed through each soil membrane, and the time required to collect the filtrate was noted to test the permeability of the membranes. The concentration of the dye before and after passing through soil membranes was determined by using a UV−vis spectrophotometer instrument (SYSTRONICS, UV−vis spectrophotometer 117). Similarly, the concentrations of the cations were determined by employing a flame photometer instrument (Analab, μFlameCal10).

Permeability of the membranes were calculated by employing the equation

$$\text{Permeability} = \frac{(\text{membrane thickness}) \times (\text{amount of permeate})}{(\text{membrane surface area}) \times (\text{time}) \times (\text{differential pressure})} \quad (3)$$

4.7. Characterization. Fourier transform infrared spectroscopy (PerkinElmer spectrum two) was employed to characterize the functional groups present in HAs. The morphology of HAs and the exfoliated vermiculite layers were characterized by FESEM (Zeiss, Model: Sigma), transmission electron microscopy (JEOL, JEM 2100), and atomic force microscopy (Agilent, model 5500 series). X-ray diffraction characterization was carried out by using Bruker D-205505 Cu Kα radiation (λ = 1.5406 Å). Tensile strength measurements of the soil membranes were carried out in a 5 kN electromechanical universal testing machine (make: Zwick Roell: Z005TN).

■ ASSOCIATED CONTENT

Supporting Information

The Supporting Information is available free of charge on the ACS Publications website at DOI: 10.1021/acsomega.8b03144.

Spectral data for characterization of vermiculite and HA; microscopic images to study the morphology of VM and HA; schematic representation for bending stiffness measurement, energy harvesting devices, and gas sensing setup; bar diagrams comparing bending stiffness of soil membranes in different environments; and UV−vis spectra for MB after passing through different membranes (PDF)

■ AUTHOR INFORMATION

Corresponding Author

*E-mail: k.raidongia@iitg.ac.in (K.R.).

ORCID

Gitish K. Dutta: 0000-0003-4370-5249

Kalyan Raidongia: 0000-0001-7829-7498

Author Contributions

‖J.D. and K.S. contributed equally to this work.

Notes

The authors declare no competing financial interest.

■ ACKNOWLEDGMENTS

K.R. acknowledges the Ramanujan Research grant (SB/S2/RJN-141/2014) and of the Science and Engineering Research Board (SERB), India for financial support. All the authors thank the Central Instrumental Facility (CIF), IIT, Guwahati, for their help with sample characterizations. J.D. acknowledges Parimita Sarma for the help with ion and dye permeation studies. J.D., K.S., R.K.G., and T.J.K. are grateful to IITG for PhD fellowships.

■ REFERENCES

(1) Evangelou, V. P. *Environmental Soil and Water Chemistry: Principles and Applications*; John Wiley & Sons: New York, 1998; pp 476−498

(2) Manahan, S. E. *Fundamentals of Environmental Chemistry*, 2nd ed.; CRC Press LLC, 2001.

(3) Wang, Y.; Wu, C.; Wang, X.; Zhou, S. The role of humic substances in the anaerobic reductive dechlorination of 2,4-dichlorophenoxyacetic acid by Comamonas koreensis starin CY01. *J. Hazard. Mater.* **2009**, *164*, 941−947.

(4) Zhou, S.; Chen, S.; Yuan, Y.; Lu, Q. Influence of humic acid complexation with metal ions on extracellular electron transfer activity. *Sci. Rep.* **2015**, *5*. DOI: 10.1038/srep17067

(5) Zhou, J. L.; Rowland, S. J.; Braven, J.; Mantoura, R. F. C.; Harland, B. J. Tefluthrin sorption to mineral particles: Role of particle organic coatings. *Int. J. Environ. Anal. Chem.* **1995**, *58*, 275−285.

(6) Boyd, S. A.; Sheng, G.; Teppen, B. J.; Johnston, C. T. Mechanisms for the adsorption of substituted nitrobenzenes by smectite clay. *Environ. Sci. Technol.* **2001**, *35*, 4227−4234.

(7) Wang, K.; Xing, B. Structural and sorption characteristics of adsorbed humic acid on clay minerals. *J. Environ. Qual.* **2005**, *34*, 342−349.

(8) Bortnikov, N. S.; Novikov, V. M.; Soboleva, S. V.; Savko, A. D.; Boeva, N. M.; Zhegallo, E. A.; Bushueva, E. B. The role of organic matter in the formation of fireproof clay of the Latnenskoe deposit. *Dokl. Earth Sci.* **2012**, *444*, 634−638.

(9) Refaey, Y.; Jansen, B.; El-Shater, A.-H.; El-Haddad, A.-A.; Kalbitz, K. The Role of Dissolved Organic Matter in Adsorbing Heavy Metals in Clay-Rich Soils. *Vadose Zone J.* **2014**, *13*. DOI: 10.2136/vzj2014.01.0009

(10) Laura, E.; McAllister, K. T. S. *Role of Clay and Organic Matter in the Biodegradation of Organics in Soil*; Springer: Dordrecht, 2010.

(11) Murray, H. H. Overview — clay mineral applications. *Appl. Clay Sci.* **1991**, *5*, 379−395.

(12) Shao, J.-J.; Raidongia, K.; Koltonow, A. R.; Huang, J. Self-Assembled two-dimensional nanofluidic proton channels with high thermal stability. *Nat. Commun.* **2015**, *6*, 7602.

(13) Gogoi, R. K.; Saha, K.; Deka, J.; Brahma, D.; Raidongia, K. Solvent-driven responsive bilayer membranes of clay and graphene oxide. *J. Mater. Chem. A* **2017**, *5*, 3523−3533.

DOI: 10.1021/acsomega.8b03144
ACS Omega 2019, 4, 1292−1299

(14) Gogoi, R. K.; Raidongia, K. Strategic shuffing of clay layers to imbue them with responsiveness. *Adv. Mater.* **2017**, *29*, 1701164.
(15) Bitinis, N.; Hernandez, M.; Verdejo, R.; Kenny, J. M.; Lopez-Manchado, M. A. Recent advances in clay/polymer nanocomposites. *Adv. Mater.* **2011**, *23*, 5229−5236.
(16) Stevenson, F. J. *Humus Chemistry: Genesis, Composition, Reaction*; Wiley Interscience: New York, 1982.
(17) Sutton, R.; Sposito, G. Molecular structure in soil humic substances: The new view. *Environ. Sci. Technol.* **2005**, *39*, 9009−9015.
(18) Zhu, W.; Zhao, F.; Yao, J. F.; Zhang, X. Y.; Wang, H. T.; Xia, C. R.; Li, C.-Z. Humic acids as a complexible fuel for combustion synthesis of ceramic nanoparticles. *J. Am. Ceram. Soc.* **2007**, *90*, 4012−4014.
(19) Baskakov, S. A.; Lobach, A. S.; Vasil'ev, S. G.; Dremova, N. N.; Martynenko, V. M.; Arbuzov, A. A.; Baskakova, Y. V.; Volodin, A. A.; Volkov, V. I.; Kazakov, V. A.; Shul'ga, Y. M. High-Temperature Carbonization of Humic Acids and a Composite of Humic Acids with Graphene Oxide. *High Energy Chem.* **2016**, *50*, 43−50.
(20) Mendez, E. M. P.; Havel, J.; Patocka, J. Humic substances-compounds of still unknown structure: applications in agriculture, industry, environment and biomedicine. *J. Appl. Biomed.* **2005**, *3*, 13−24.
(21) Luo, W.-J.; Gao, Q.; Wu, X.-L.; Zhou, C.-G. Removal of cationic dye(methylene blue) from aquoeus solution by humic acid modified expanded perlite. *Sep. Sci. Technol.* **2014**, *49*, 2400−2411.
(22) Shenvi, S. S.; Isloor, A. M.; Ismail, A. F.; Shilton, S. J.; Ahmed, A. A. Humic acid based biopolymeric membrane for effective removal of methylene blue and rhodamine B. *Ind. Eng. Chem. Res.* **2015**, *54*, 4965−4975.
(23) Serra, M. O. D.; Schnitzer, M. Extraction of Humic Acid by Alkali and Chelating Resin. *Can. J. Soil Sci.* **1972**, *52*, 365−374.
(24) Paul, S.; Sharma, T.; Saikia, D.; Saikia, P.; Borah, D.; Baruah, M. Evaluation of pKa Values of Soil Humic Acids and their Complexation Properties. *Int. J. Plant Soil Sci.* **2015**, *6*, 218−228.
(25) Schepetkin, I. A.; Khlebnikov, A. I.; Ah, S. Y.; Woo, S. B.; Jeong, C.-S.; Klubachuk, O. N.; Kwon, B. S. Characterization and biological activities of humic substances from mumie. *J. Agric. Food Chem.* **2003**, *51*, 5245−5254.
(26) Rodrigues, A.; Brito, A.; Janknecht, P.; Proença, M. F.; Nogueira, R. Quantification of humic acids in surface water: effects of divalent cations, pH, and filtration. *J. Environ. Monit.* **2009**, *11*, 377−382.
(27) Bayer, C.; Martin-Neto, L.; Mielniczuk, J.; Saab, S. d. C.; Milori, D. M. P.; Bagnato, V. S. Tillage and cropping system effects on soil humic acid characteristics as determined by electron spin resonance and fluorescence spectroscopies. *Geoderma* **2002**, *105*, 81−92.
(28) Monsallier, J.-M.; Scherbaum, F. J.; Buckau, G.; Kim, J.-I.; Kumke, M. U.; Specht, C. H.; Frimmel, F. H. Influence of photochemical reactions on the complexation of humic acid with europium(III). *J. Photochem. Photobiol., A* **2001**, *138*, 55−63.
(29) Balcke, G. U.; Kulikova, N. A.; Hesse, S.; Kopinke, F.-D.; Perminova, I. V.; Frimmel, F. H. Adsorption of humic substances onto kaolin clay related to their structural features. *Soil Sci. Soc. Am. J.* **2002**, *66*, 1805−1812.
(30) Tombácz, E.; Libor, Z.; Illés, E.; Majzik, A.; Klumpp, E. The role of reactive surface sites and complexation by humic acids in the interaction of clay mineral and iron oxide particles. *Org. Geochem.* **2004**, *35*, 257−267.
(31) Nascimento, F. H. d.; Masini, J. C. Influence of humic acid on adsorption of Hg(II) by vermiculite. *J. Environ. Manage.* **2014**, *143*, 1−7.
(32) Zhang, L.; Luo, L.; Zhang, S. Integrated investigations on the adsorption mechanisms of fulvic and humic acids on three clay minerals. *Colloids Surf., A* **2012**, *406*, 84−90.
(33) Mark, R. E.; Habeger, C. C.; Borch, J.; Lyen, M. B. *Handbook of Physical Testing of Paper*; CRC Press, 2001.
(34) Raidongia, K.; Huang, J. Nanofluidic ion transport through reconstructed layered materials. *J. Am. Chem. Soc.* **2012**, *134*, 16528−16531.
(35) Lee, S.; Kim, H.; Kim, D.-K. Power Generation from Concentration Gradient by Reverse Electrodialysis in Dense Silica Membranes for Microfluidic and Nanofluidic Systems. *Energies* **2016**, *9*, 49−60.
(36) Ji, J.; Kang, Q.; Zhou, Y.; Feng, Y.; Chen, X.; Yuan, J.; Guo, W.; Wei, Y.; Jiang, L. Osmotic power generation by positively and negatively charged 2D nanofluidic membrane pairs. *Adv. Funct. Mater.* **2016**, *27*, 1603623.
(37) Bayer, T.; Bishop, S. R.; Perry, N. H.; Sasaki, K.; Lyth, S. M. Tunable mixed ionic/electronic conductivity and permittivity of graphene oxide paper for electrochemical energy conversion. *ACS Appl. Mater. Interfaces* **2016**, *8*, 11466−11475.

DOI: 10.1021/acsomega.8b03144
ACS Omega 2019, 4, 1292−1299